

Enhanced ultraviolet photocatalytic activity of Ag/ZnO nanoparticles synthesized by modified polymer-network gel method

Y. H. Lu · M. Xu · L. X. Xu · C. L. Zhang · Q. P. Zhang ·
X. N. Xu · S. Xu · K. Ostrikov

Received: 8 May 2015 / Accepted: 10 August 2015 / Published online: 29 August 2015
© Springer Science+Business Media Dordrecht 2015

Abstract Ag/ZnO nanoparticle (NP) heterostructures are synthesized through a modified polymer-network gel method in which glucose is added to the precursor solution to prevent the gel from drastically shrinking during drying of the aqueous solution. Structural and optical properties of the samples are characterized by a range of techniques including XRD, SEM, TEM, XPS, UV–Vis, and PL. The high-quality Ag–ZnO heterostructure is evidenced clearly by high-resolution TEM. The Ag/ZnO heterostructure nanocomposites exhibit a higher photocatalytic activity in the degradation of

methyl orange than pure ZnO. Especially, Ag/ZnO NP heterostructures with the Ag/Zn molar ratio of 5:95 (sample ZA-5) show the highest degradation efficiency, which is 11 times higher compared with pure ZnO. The photoluminescence properties of the heterostructures and O defect states are studied to well explain the observed photocatalytic effects. ZA-5 also exhibits competitive photocatalytic activity for the degradation of other pollutant dyes such as Methylene blue and Rhodamine B compared with the recently reported techniques, while showing excellent catalyst photostability as well as offering simplicity and reliability.

Y. H. Lu · M. Xu (✉) · C. L. Zhang ·
Q. P. Zhang · X. N. Xu
Key Laboratory of Information Materials of Sichuan
Province, School of Electrical and Information
Engineering, Southwest University for Nationalities,
Chengdu 610041, China
e-mail: hsuming_2001@aliyun.com

L. X. Xu · S. Xu
Plasma Sources and Applications Center, NIE, Nanyang
Technological University, Singapore 637616, Singapore

K. Ostrikov (✉)
Institute for Future Environments and School of
Chemistry, Physics, and Mechanical Engineering,
Queensland University of Technology, Brisbane,
QLD 4000, Australia
e-mail: kostya.ostrikov@qut.edu.au

K. Ostrikov
Plasma Nanoscience Laboratories, Industrial Innovation
Program, Manufacturing Flagship, CSIRO,
P. O. Box 218, Lindfield, NSW 2070, Australia

Keywords Photocatalysis · Ag/ZnO
heterostructures · Nanocomposite · Polymer-network
gel method

Introduction

Rapid expansion of textile industries has led to major water pollution by industrial waste such as inorganic and organic dyes. Common wastewater treatments are based on adsorption (Sauer et al. 2002; Wang et al. 1998), reverse osmosis (Tünay et al. 1996), chemical coagulation (Galindo et al. 2001), and other techniques. However, these methods are somewhat inefficient because they require further treatments and the operating costs are quite high. Semiconductor-assisted photochemical processing is promising for treating various water pollutants (Fockede and Van Lierde

2002). It offers high degradation capacity based on effective oxidation of contaminants, which leads to relatively simple and low-cost processes for the destruction of toxic and treatment-resistant substances.

Some oxide semiconductors, such as TiO_2 , ZnO , SnO_2 , and WO_3 , can effectively degrade most of the organics to CO_2 , H_2O , and inorganic ions under UV irradiation. In particular, ZnO or TiO_2 are widely considered as promising materials for purification and disinfection of water and air, owing to their high activity, environment friendliness, and relatively low cost. Recent reports suggest that ZnO could be even more effective than TiO_2 in the selected photocatalytic reactions (Kozlov et al. 2000; Khodja et al. 2001; Dias and Azevedo 2009; Kositzi et al. 2004; Gouvea et al. 2000).

Nanometer-sized ZnO has a larger specific surface area-to-volume ratio which leads to better photocatalytic performance compared with bulk ZnO (Sin et al. 2014; Kajbafvala et al. 2012). However, the rates of recombination of photoinduced electrons and holes remain high which limits practical applications of ZnO nanoparticles.

Deposition of noble metal nanoparticles on the semiconductor is a promising means to overcome this limitation. The mechanism of this improvement is based on the conducting band (CB) electron transfer to the metal nanoparticles, which act as electron collectors due to the Schottky barrier at the metal–semiconductor interface. On the other hand, the photogenerated holes remain at the semiconductor surface. Moreover, the nanoparticles also change the defect concentrations in the semiconductor thereby enhancing the photocatalytic efficiency (Lu et al. 2008a, b; Zheng et al. 2008).

It was suggested that the presence of the hydroxyl groups and defects on the surface may change photocatalytic redox reactions, and consequently, the photocatalytic efficiency (Zhang et al. 2014a, b; Wang et al. 2012a, b); however, the available results to confirm these effects are quite limited. This work suggests that Ag nanoparticles not only act as electron sinks to enhance the separation of the photoinduced electrons from holes, but also change the concentrations of defects to elevate the amount of surface hydroxyl radicals.

On the other hand, much effort has been devoted to the synthesis of Ag/ ZnO heterostructures with tunable morphological and structural parameters to effectively

degrade various pollutants in wastewater (Xu et al. 2008; Guo et al. 2013; Divband et al. 2013; Wang et al. 2012a, b). Diverse synthesis routes including conventional hydrothermal, sol–gel, and wet chemical methods have been developed to synthesize Ag/ ZnO photocatalysts (Lu et al. 2008a, b; Guo et al. 2013; Chai et al. 2014; Zhang and Mu 2007; Yin et al. 2012; Zheng et al. 2007; Karunakaran et al. 2011). However, these methods commonly involve several stages (e.g., post-process purification) and complex reaction initiators, require significant water resources and sophisticated equipment, as well as suffer from high cost and limited industrial scalability. Importantly, particle agglomeration has been identified as one of the most critical issues because it dramatically reduces the surface area-to-volume ratio of the catalyst thereby significantly diminishing the photocatalytic activity (Sin et al. 2014; Lu et al. 2008a, b; Saravanan et al. 2013).

Here we present an efficient and economic way to synthesize Ag/ ZnO crystalline heterostructures featuring high photocatalytic efficiency and stability. The modified polyacrylamide gel method is used to synthesize almost spherical, near-size-uniform and non-agglomerated nanoparticles (Liu et al. 2007; Han et al. 2013; Wang et al. 2013a, b, c; Xian et al. 2009; Zhang et al. 2011; Lin et al. 2012; Wang et al. 2014; Douy 2001). Transmission electron microscopy reveals a clear heterojunction interface and good crystalline order indicating strong bonding between Ag nanoparticles and ZnO nanocrystals. This leads to the enhanced stability and performance in photocatalytic degradation of the common pollutant dyes such as Methyl Orange (MO), Methylene Blue (MB), and Rhodamine B (RhB).

Table 1 suggests that our Ag/ ZnO heterostructures show competitive performance compared with the recently reported techniques (Xu et al. 2008; Guo et al. 2013; Zhang and Mu 2007; Yin et al. 2012; Zhu et al. 2014), while showing excellent catalyst photostability as well as offering simplicity and reliability. These factors are crucial for the scaled industrial production of nanocrystalline Ag/ ZnO heterostructure-based photocatalysts. Our versatile, simple, cheap, and environment-friendly synthesis approach may also be applicable for the controlled and scaled productions of other metal/metal-oxide nanocomposite materials for diverse applications in chemical catalysis, energy, health, and other fields.

Table 1 Photocatalytic activity of Ag/ZnO system

Dye	High-pressure mercury lamp (W)	Initial dye conc.	Catalyst concentration (g/L)	Time for complete degradation (min)	Ref.
MO	300	20 mg/L	0.3	90	Yin et al. (2012)
RhB	300	1×10^{-5} mol/L	1	15	Zhang and Mu (2007)
RhB	250	1×10^{-5} mol/L	0.2	>50	Zhu et al. (2014)
RhB	250	5×10^{-5} mol/L	0.5	100	Guo et al. (2013)
RhB	300	1×10^{-5} mol/L	1	>20	Xu et al. (2008)
MO	250	1.22×10^{-5} mol/L	0.5	25	This work
MB		1.06×10^{-5} mol/L	0.5	30	
RhB		1×10^{-5} mol/L	0.2	45	

Experimental

Catalyst preparation

All reagents are of analytic grade and used as received without further purification. The reagents include zinc nitrate, argentum nitricum, tartaric acid, glucose, acrylamide, *N,N'*-methylene bisacrylamide, and deionized water.

The synthesis process of Ag/ZnO nanoparticle heterostructures via the polyacrylamide gel method is described as follows. In a typical synthesis process, 10 mmol metal salt with various mole ratios ($n(\text{Zn}(\text{NO}_3)_2)/n(\text{AgNO}_3) = 0, 1:99, 3:97, 5:95, 8:92$) was dissolved in 30 mL distilled water at room temperature. After the solution was clear and without residue, tartaric acid was added to the solution in the molar ratio 1.5:1 with respect to the cations. Subsequently, about 20 g glucose was dissolved. Finally, the acrylamide utilized as monomer and *N,N'*-methylene-bisacrylamide used as lattice reagent were added to the solution. The mass ratio between monomer and lattice reagent was 5:1. The total amount of the used acrylamide and *N,N'*-methylene-bisacrylamide was 9 times the amount (mole) of the cations.

Every step mentioned above was accompanied by constant magnetic stirring to make the solution transparent and uniform. The resultant solution was heated at 90 °C to initiate the polymerization reaction, and about 10 min later a polyacrylamide gel was formed. The gel was dried at 120 °C for 24 h in a thermostat drier. The obtained xerogel was ground into a fine powder in an agate mortar, and then calcinated at 650 °C for 5 h in a tube furnace. The samples produced were labeled as ZA-0, ZA-1, ZA-3, ZA-5, and ZA-8, corresponding to the different mole

ratios of $\text{Zn}(\text{NO}_3)_2$ to AgNO_3 at 0, 1:99, 3:97, 5:95, 8:92, respectively.

Materials characterization

X-ray diffraction patterns (XRD) were collected using an X'pert pro MPD diffractometer with $\text{Cu}_{K\alpha}$ radiation ($\lambda = 1.5418 \text{ \AA}$ and $\theta = 20\text{--}80^\circ$) at room temperature. The morphologies of the as-prepared samples were examined by a field emission scanning electron microscope (JSM-7500F produced by JEOL). Transmission Electron Microscopy (TEM) and High-resolution TEM (HRTEM) were performed on a Tecnai G² F20 microscope at 200 kV electron beam energy.

The surface chemical composition was determined by X-ray photoelectron spectroscopy (XPS). The measurements were performed in a VG Scientific ESCALAB 210 spectrometer equipped with an Mg anode and the source power of 300 W. All the binding energies were calibrated with respect to the C 1s peak at 285.0 eV. The fitting of XPS peaks was performed using Origin 7.0 software.

Photoluminescence (PL) spectra were obtained at room temperature by RF-5310pc fluorescence spectrophotometer with the excitation wavelength 325 nm. The solid samples were dispersed in water and UV-Vis spectra were measured from these dispersions using an UNICAM-UV500 spectrophotometer to detect absorption over the range of 200–800 nm.

Photocatalytic activity

The photocatalytic performance of the samples was evaluated by the degradation of methyl orange (MO) used as a representative pollutant dye. For each condition, 0.05 g catalyst and 100 mL of 4 mg/L

MO aqueous solution was mixed in a 250 mL beaker. Photocatalyst was ultrasonically dispersed in MO aqueous solution and magnetically stirred in the dark to ensure the adsorption/desorption equilibrium of MO with the catalyst. In detail, after stirring in the dark for 5 min, the beaker with the above solution was put into an ultrasonic bath.

After ultrasonic treatment for 3 min at room temperature, the solution was left in the dark environment for 30 min to establish adsorption equilibrium of the dye on the catalyst surface. The solution was then exposed to the high-pressure mercury lamp (Philips HPL-N 250 W). After a given irradiation time, 4.5 mL of the mixture in the beaker was removed and then centrifuged to separate the residual catalyst. The V-1100D spectrometer was used to measure the concentration of MO solution before and after the photocatalytic reaction. The photocatalytic activity was evaluated following the procedures described elsewhere (Tünay et al. 1996).

Results and discussion

XRD analysis

The XRD patterns of the as-synthesized pure ZnO and Ag/ZnO heterostructures with different Ag/Zn molar ratios are presented in Fig. 1. All the spectra clearly show the (100), (002), (101), (102), (110), (103),

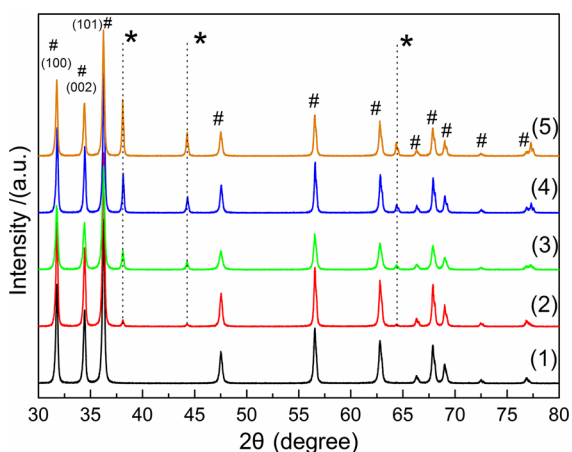


Fig. 1 XRD spectra of pure ZnO (1) and Ag/ZnO nanoparticle heterostructures with different Ag/Zn molar ratios: (2) 1:99, (3) 2:98, (4) 5:95, and (5) 8:92

(200), (112), and (201) peaks characteristic to the hexagonal structure of ZnO. The patterns of Ag/ZnO heterostructures with different Ag/Zn molar ratios exhibit two sets of strong diffraction peaks, indicating that the as-synthesized products are composite materials. Those marked with “#” can be attributed to hexagonal wurtzite ZnO (JCPDS file no. 79-0208), while the others marked with “*” can be indexed to face-centered-cubic (*fcc*) metallic Ag (JCPDS file no. 89-3722). The intensity of silver peaks in the nanocomposite samples increase with the increase in the amount of Ag. This suggests that silver preserves its metallic form in the Ag/ZnO nanocomposite. The crystallite size of the samples was calculated by using the Scherer’s equation. The lattice parameters and the crystallite sizes of the samples are shown in Table 2.

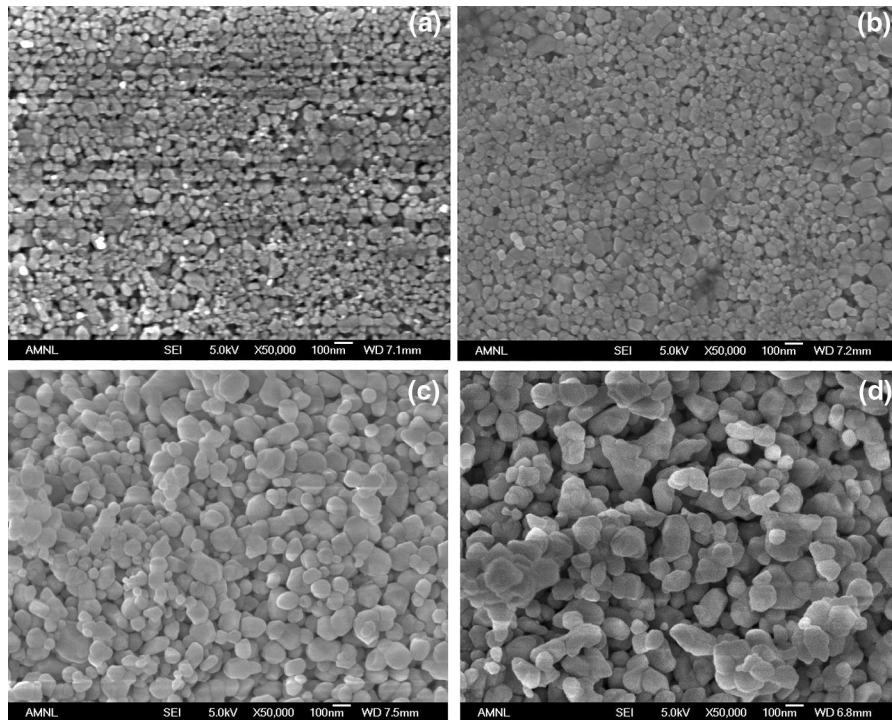
SEM analysis

SEM and TEM microscopic methods were used to characterize the morphologies and microstructures of ZnO particles and Ag/ZnO composites. The SEM image in Fig. 2a reveals that ZnO particles have a nearly spherical shape with the diameter ranging from 10 to 40 nm. It is also seen that the particles are polydisperse and are not agglomerated. Figure 2c clearly shows that nanoparticles in ZA-5 also have the smooth near-spherical shape with a fairly uniform diameter around 40 nm. These particles are also polydisperse and not agglomerated. With the change of the Ag/Zn molar ratio to 8:92, the diameter of Ag/ZnO nanoparticles becomes larger. An interesting observation was made that addition of AgNO₃ does not significantly affect the morphology of ZnO. Thus, the addition of AgNO₃ influences the size of ZnO by its involvement in the uniform nucleation and scalable growth, which preserves the nanoparticle shape (Saravanan et al. 2013).

Figure 3 shows the TEM images of the Ag/ZnO nanoparticle heterostructures with Ag/Zn molar ratios 5:95. The micrographs confirm the high quality of the heterostructures made of metallic Ag nanoparticles and ZnO nanoparticles. From Fig. 3a and b, one can also see that the silver nanoparticles are loaded on the irregularly oriented ZnO nanocrystals. Figure 3c is a high-resolution TEM (HRTEM) image taken from the squared region of Fig. 3a. Two kinds of lattice spacing and a well-resolved and smooth interface are observed. The plane fringe with a crystalline plane

Table 2 Lattice parameters and crystallite sizes of pure ZnO and Ag/ZnO heterostructures with different Ag/Zn molar ratios

Sample	ZnO Hexagonal 79-0208			Ag Cubic 89-3722	
	<i>a</i> /nm	<i>c</i> /nm	Crystallite size/nm	<i>a</i> /nm	Crystallite size/nm
ZA-0	0.32516	0.5211	34.1	–	–
ZA-1	0.32506	0.5210	36.4	0.40896	48.8
ZA-3	0.32526	0.5206	29.7	0.40886	41.1
ZA-5	0.32486	0.5209	37.7	0.40855	45.4
ZA-8	0.32526	0.5206	38.8	0.40896	48.7

**Fig. 2** SEM images of pure ZnO (a) and Ag/ZnO heterostructures with different Ag/Zn molar ratios: b 1:99, c 5:95, and d 8:92

spacing of 0.236 nm is assigned to the (111) plane of Ag with *fcc* structure. The other plane spacing of 0.256 nm corresponds to (002) planes of wurtzite ZnO. These results demonstrate that Ag nanoparticles in the Ag/ZnO composites have *fcc* structure (Lu et al. 2008a, b; Zheng et al. 2007; Zhang et al. 2014a, b; Yang et al. 2011; Dinesh et al. 2014), while ZnO crystals are of wurtzite structure, in a good agreement with the XRD results.

In Fig. 3a, one can observe some darker granular areas of ZA-5 sample, which may possibly be attributed to the presence of larger Ag particles. However, other factors, such as extinction, can also lead to the observation of some darker granular areas,

when TEM is used to characterize the morphology of nanoparticles. The darkness/contrast depends on the relative orientations of the electron beam direction and the crystalline grains, which is also possible for non-agglomerated Ag particles.

XPS analysis

To examine the elemental and surface chemical state of Ag/ZnO samples, the XPS analysis was performed. In Fig. 4a, all of the peaks on the curve are ascribed to Zn, Ag, O, and C elements, and no peaks for other elements are observed. The presence of C is likely because of the pump oil residues during the vacuum

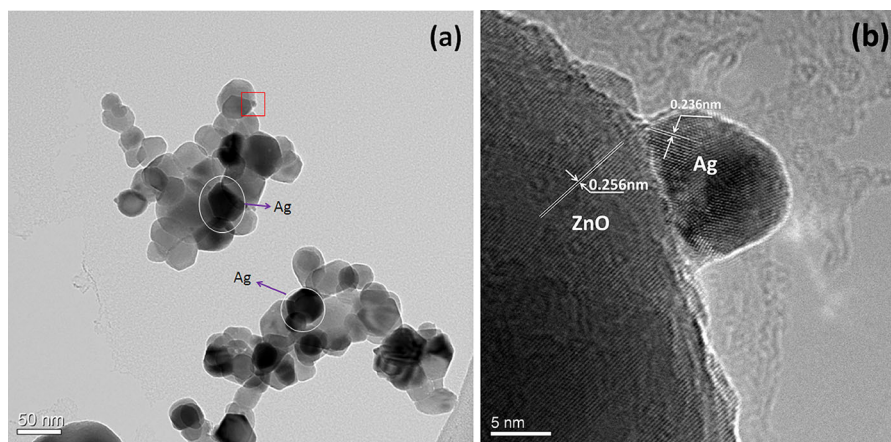


Fig. 3 TEM images of the as-synthesized Ag/ZnO nanoparticle heterostructures with the Ag content of 5 at. %: **a** low-magnification TEM image; **b** HRTEM image from the *squared* region of **(a)**

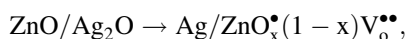
treatment before the XPS analysis. As shown in Fig. 4b, the Zn $2p_{3/2}$ and Zn $2p_{1/2}$ XPS spectra are observed in ZA-0, ZA-1, ZA-5, and ZA-8 samples at around 1021.6 eV and 1044.3 eV, respectively. This indicates that Zn element is mainly present in the samples in the form of Zn^{2+} (Chai et al. 2014).

Figure 4c shows the Ag $3d_{5/2}$ and Ag $3d_{3/2}$ XPS spectra of ZA-1, ZA-5, and ZA-8 samples, which are peaked at 367.5 and 373.4 eV, respectively. The binding energies (BEs) of Ag $3d_{5/2}$ and Ag $3d_{3/2}$ for each Ag/ZnO sample shift to lower values compared with the BE of pure Ag nanoparticles (the standard binding energies of Ag $3d_{5/2}$ and Ag $3d_{3/2}$ states for bulk Ag are about 368.2 and 374.2 eV, respectively (Zheng et al. 2007; Saravanan et al. 2013)).

The electron density of Ag decreases because of the transfer of electrons from the Ag nanoparticles to ZnO nanoparticles. The binding energy of monovalent Ag is much lower than that of zero-valent Ag. The electron density of Ag becomes smaller if the Ag nanoparticle is put into contact with ZnO. The work functions of ZnO and Ag are 5.2 eV and 4.26 eV, respectively (Saravanan et al. 2013; Zhang et al. 2014a, b). As such, the Fermi energy level of Ag (E_{fm}) is higher than that of ZnO (E_{fs}). It is thus possible that free electrons transfer from Ag to ZnO until the two systems attain the new and balanced Fermi energy level (E_f). Furthermore, in our experiment, the BE value of Ag in the Ag/ZnO nanoparticle heterostructures is even slightly lower compared with pure Ag, indicating the strong interaction between Ag and ZnO nanoparticles.

Figure 5 shows the deconvoluted XPS spectra of O $1s$ states in the nanoparticle heterostructure samples with different loading of Ag nanoparticles. It can be seen that the O $1s$ peaks are quite asymmetric in all the samples, suggesting that there are at least two kinds of bonding states of oxygen species on the surface. The O $1s$ spectra of the ZnO samples can be described as the superposition of three peaks by Gaussian distribution, located around 530.3, 531.5, and 532.3 eV (Zhang et al. 2014a, b; Wang et al. 2012a, b). These peaks are associated with O^{2-} species in the lattice (O_L), oxygen vacancies or defects (O_V), and chemisorbed or dissociated (O_C) oxygen species, respectively (Zhang et al. 2014a, b; Wang et al. 2012a, b).

It is suggested that the variation of the oxygen defect concentration on the surface of ZnO nanocrystals should be related to the interface between Ag nanoparticles and ZnO nanoparticles and the surface-to-volume ratio of ZnO nanoparticles (Zheng et al. 2008). The chemical reaction process for the generation of Ag/ZnO heterostructure nanocrystals is proposed as follows:



where $x < 1$. As mentioned above, ZnO and Ag_2O are connected through a Zn–O–Ag bond in the early stage of the sintering process. During the high temperature sintering process, organics is reduced gradually, and a Zn–O–Ag bond should be formed between metallic Ag and ZnO nanocrystals, resulting in the formation of Ag/ZnO heterostructure nanocrystals with a strong

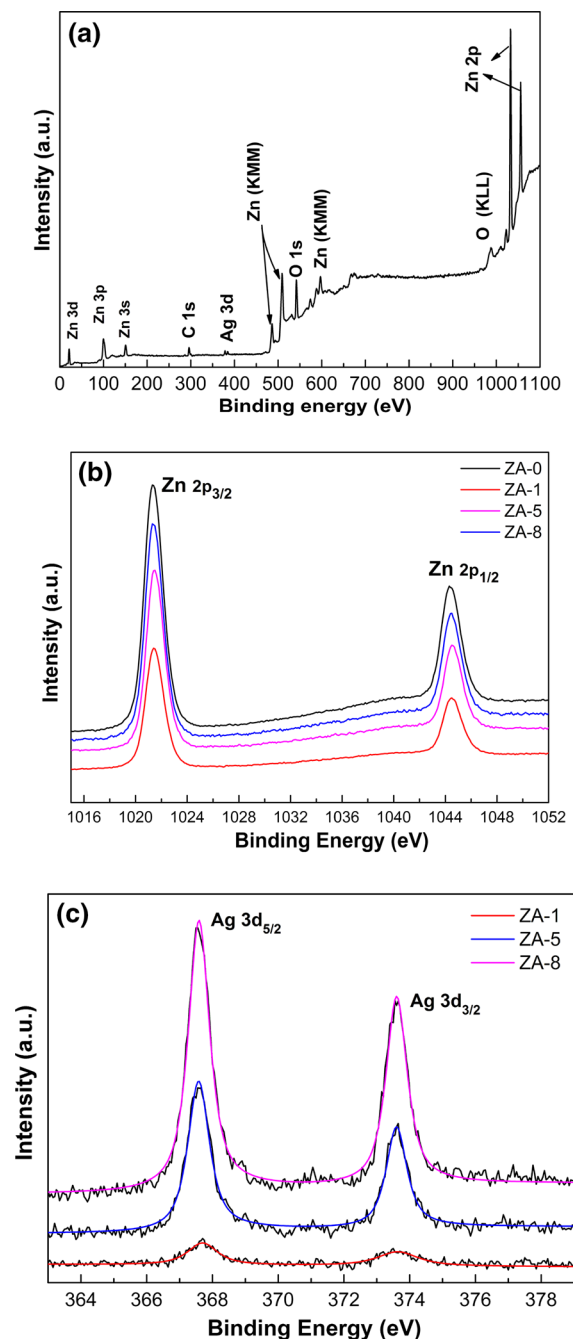


Fig. 4 **a** Representative XPS survey spectrum of Ag/ZnO sample with the Ag content of 5 at.%. The XPS full spectra of **b** Zn 2p and, **c** Ag 3d states of the as-prepared Ag/ZnO samples with different Ag contents

interaction. In other words, the addition of AgNO₃ to the reaction system can lessen the crystallinity and increase the percentage of hydroxyl oxygen of ZnO. The concentration of oxygen defect for the as

synthesized samples varies with the increasing Ag content. The Ag/ZnO sample with the Ag content of 5.0 at.% has the largest density of oxygen defects. When the amount of Ag nanoparticles exceeds 5.0 at.%, the grain size of Ag/ZnO nanocrystals increases further as revealed by the XRD results, leading to a decrease of the oxygen defect concentration.

Since the varying oxygen defect concentrations and types of defects play a crucial role in trapping photoinduced electrons and holes, the quantitative analysis of O 1s XPS spectra has been carried out, and the results are summarized in Table 3. According to the results, the O_V (531.5 eV) value of O 1s is higher for the Ag/ZnO nanoparticle heterostructures with Ag/Zn molar ratios 5:95 (ZA-5). Some author groups observed the significant surface hydroxyl signals in the XPS full spectra of O 1s states of the Ag/ZnO samples (Lu et al. 2008a, b) due to the presence of hydroxyl groups bonded to surface defects on ZnO (Zhang et al. 2014a, b). The hydroxyl groups detected by XPS are associated with surface defects on ZnO samples. It can be seen that, as the Ag content increases, the surface hydroxyl content first increases and then decreases, reaching the maximum value at 5 at.% of Ag.

Photoluminescence spectra

It is well known that exposure of semiconductor nanocrystals to photons with the energy above the bandgap energy leads to the formation of electron–hole pairs: electrons in the conduction band (CB) and holes in the valence band (VB). A few of such electron–hole pairs diffuse into the crystal surface and react with the adsorbed species, resulting in photocatalytic reactions (Karunakaran et al. 2011). The photoluminescence (PL) signals result from the recombination of photoinduced charge carriers in the semiconductor materials (Hong et al. 2013). Therefore, the PL intensity is related to the photocatalytic activity. This is the reason that we carried out the PL measurements under UV irradiation with the wavelength of 325 nm at room temperature. This study provides the information about the efficiency of charge carrier trapping, migration and transport, as well as the presence of surface defects and oxygen vacancies.

It can be seen in Fig. 6 that the four spectra of the Ag/ZnO nanospheres display three similar main emission bands. The band around 390 nm (closest to the UV excitation wavelength) can be ascribed to the

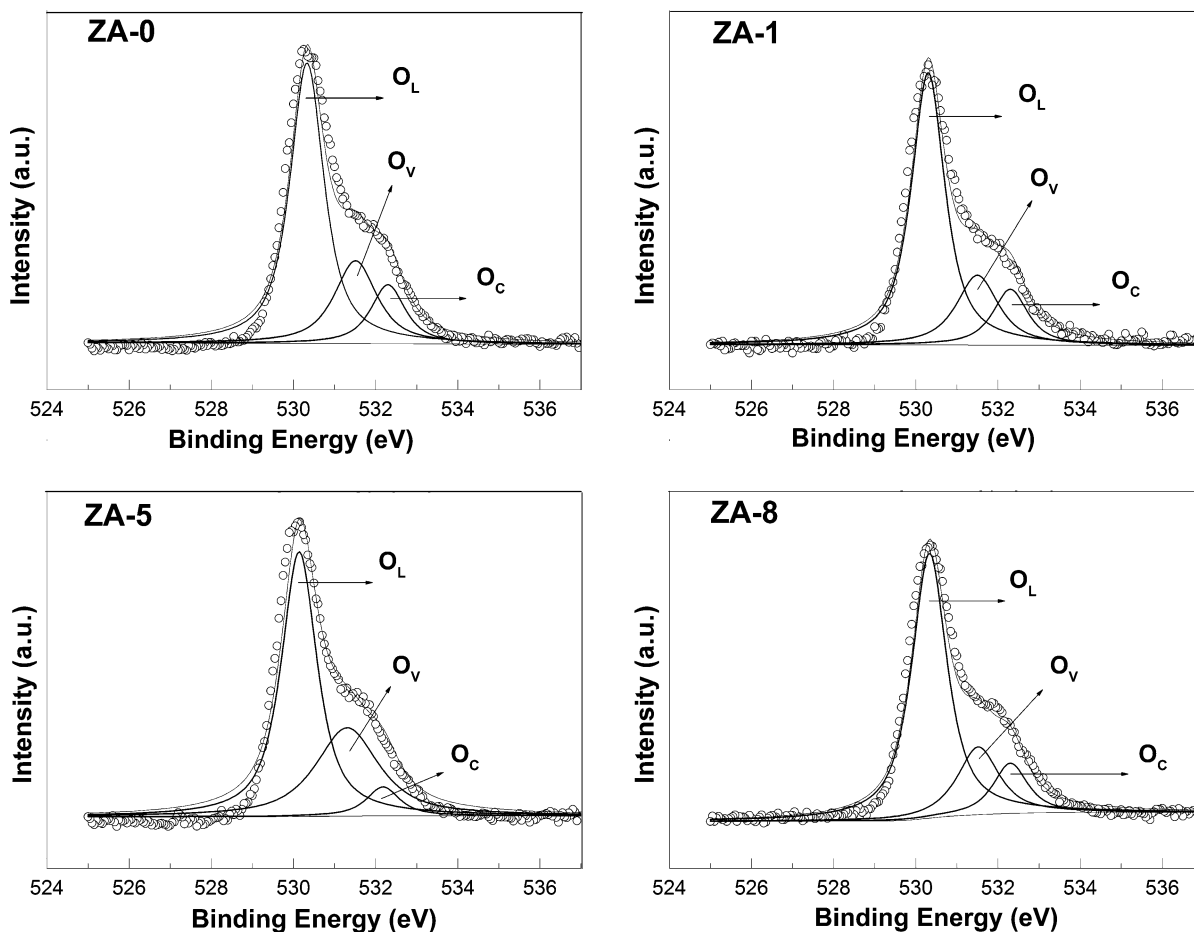


Fig. 5 The XPS spectra of O $1s$ states of pure ZnO and Ag/ZnO nanoparticle heterostructures with different Ag/Zn molar ratios

recombination of excitonic centers. Another fairly weak and broad band corresponds to blue emission at 475 nm, which may originate from bound excitons (Jing et al. 2006). The weak green band at 525 nm was also observed.

A number of hypotheses have been proposed to explain the green emission, including transition between an electron close to the conduction band and a deeply trapped hole at Vo^{++} , surface defects like Zn^{2+} vacancies, transition between antisite oxygen and donor–acceptor complexes and some others (Jing et al. 2006; Georgekutty et al. 2008). Such long-wavelength emission may also be due to the recombination of photogenerated holes with the singly ionized oxygen vacancy site (Jing et al. 2006; Vanheusden et al. 1996). Since that former case is quite rare, hole interactions with the oxygen vacancies may thus be a more probable cause for the emission.

The UV emission intensity of the Ag/ZnO nanospheres is lower compared with ZnO nanospheres. This may be attributed to the formation of heterostructures of Ag and n-type semiconductor ZnO. Moreover, it can be seen that the sample ZA-5 shows the minimum PL intensity. As the Ag content increases, the PL intensity of the Ag/ZnO nanoparticle heterostructures does not decrease monotonously.

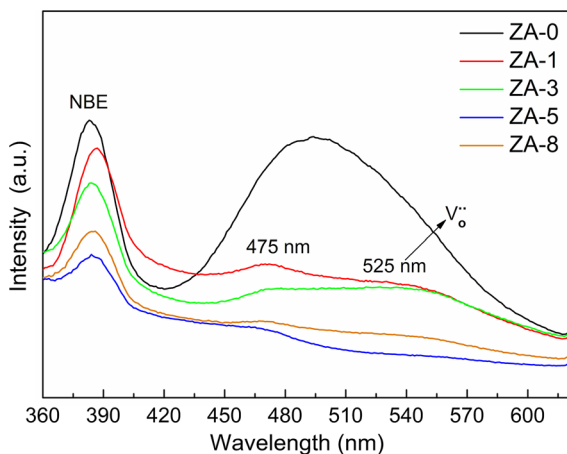
The PL intensity of each emission band of ZnO loaded with Ag is lower than that of ZnO nanospheres. This observation may be attributed to the effect of the Ag deposits which did not act as electron sinks to enhance the separation of photoinduced electrons from holes.

With the increasing Ag content (e.g., sample ZA-5), more metal sites are formed to become available to accept electrons. This leads to better separation of the photoinduced electrons and holes, and consequently, to a further decrease of PL emission.

Table 3 Analyses of O 1s XPS spectra of pure ZnO and Ag/ZnO nanoparticle heterostructures with different Ag/Zn molar ratios

Sample	O_L	O_V	O_C
ZA-0			
E_b (eV)	530.3	531.5	532.3
FWHM (eV)	0.98	1.23	1.00
R_i %	63.06	23.39	13.54
ZA-1			
E_b (eV)	530.3	531.5	532.3
FWHM (eV)	0.97	1.21	1.01
R_i %	65.22	20.86	13.91
ZA-5			
E_b (eV)	530.2	531.3	532.2
FWHM (eV)	1.03	1.81	0.95
R_i %	59.24	34.76	5.99
ZA-8			
E_b (eV)	530.3	531.5	532.3
FWHM (eV)	1.02	1.19	1.00
R_i %	67.34	20.11	12.5

FWHM full width at half maximum, R_i % the percent of the individual oxygen species calculated from the peak area

**Fig. 6** PL spectra of pure ZnO and Ag/ZnO nanoparticle heterostructures with different Ag/Zn molar ratios excited at 325 nm

However, when the Ag content exceeds a certain value (e.g., sample ZA-8), the PL intensity increases. There is a possibility that Ag nanoparticles (NPs) deposited on the ZnO NPs can aggregate and become larger. It was suggested that this aggregation may reduce the number of effective traps for photoelectrons, and

consequently, enhance the PL intensity (Yao et al. 2002).

However, based on the average diameter of Ag nanoparticles obtained from our XRD results (Fig. 1), the size of Ag NPs does not change significantly. Therefore, the enhanced PL may be attributed to a significant decrease in the specific surface areas of Ag/ZnO nanoparticles (according to our SEM measurements, Fig. 2), which reduces light absorption (Saranvanan et al. 2013).

In addition, when the metal nanoparticle loading is above the optimum level, over-accumulation of electrons on the metal surface could attract the photo-generated holes to the metal sites. This may in turn enhance the recombination of the charge carriers, and consequently, the PL intensity observed in the experiments.

Importantly, our results suggest that higher excitonic PL intensities correspond to weaker photocatalytic activity, and vice versa. This relationship is consistent with the results of other authors (Hong et al. 2013; Xin et al. 2005; Ren et al. 2010; Sun et al. 2012a, b).

UV–Vis spectra

The UV–Vis spectra of nanocomposites with different Ag concentrations are presented in Fig. 7. The ZnO nanostructure and Ag/ZnO nanocomposites exhibit strong absorption in the UV region with the peak at ~ 375 nm. The bandgap energy was calculated to be 3.29 eV as labeled in Fig. 7. Loading of Ag nanoparticles on ZnO did not cause any significant change in the ZnO bandgap energy. However, when the amount of deposited Ag on the ZnO surface is increased, the ultraviolet absorption peak of Ag–ZnO heterostructure at 377 nm becomes broader. The enhanced light absorption can thus provide more photoelectrons for photocatalytic reactions (Zhu et al. 2014; Sun et al. 2012a, b; Bai et al. 2013).

Surface photovoltage spectroscopy

Surface photovoltage spectroscopy (SPS) is a well-established contactless and nondestructive technique for semiconductor characterization that relies on analyzing illumination-induced changes in the surface voltage (Su et al. 2008; Li et al. 2009). As is known, SPS presents the surface photovoltage (SPV) amplitude as a function of the incident wavelength. This tool

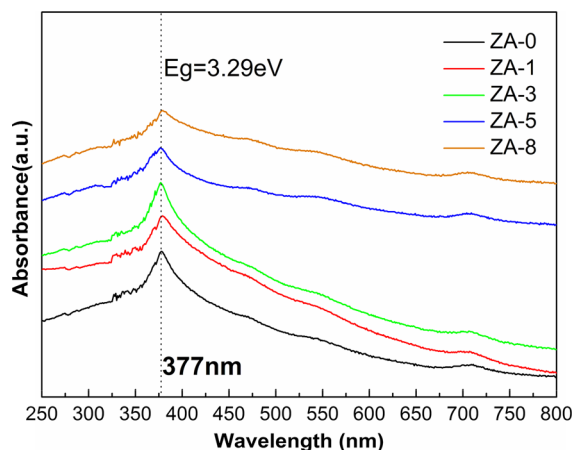


Fig. 7 UV-Visible absorption spectra of pure ZnO and Ag/ZnO nanoparticle heterostructures with different Ag/Zn molar ratios

was also effective for the investigation of the photoinduced charge-transfer properties in our Ag/ZnO system and may provide useful information for understanding the UV-light catalytic mechanism of the sample. The results of surface photovoltage spectroscopy (SPS) of the samples are shown in Fig. 8. The strong SPS response peak at 380 nm observed on Ag/ZnO can be attributed to the electron transition from the valence band to the conduction band of ZnO. This demonstrates that the generated electron-hole pairs could be separated effectively under the irradiation of UV-light. In contrast with pure ZnO, Ag/ZnO heterostructure nanocrystals exhibit much stronger SPV response. Interestingly, the

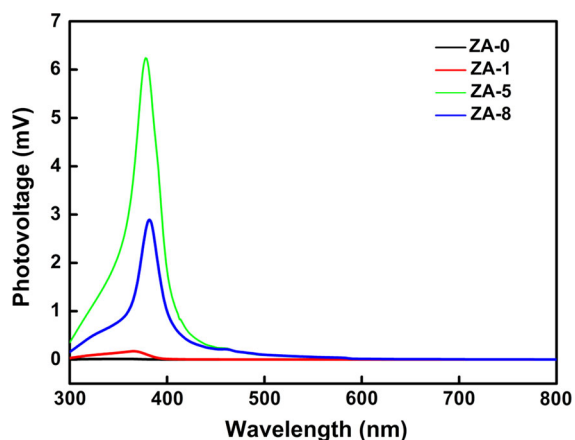


Fig. 8 SPS of pure ZnO and Ag/ZnO nanoparticle heterostructures with different Ag/Zn molar ratios

strongest SPV response for the Ag/ZnO heterostructure nanocrystals with 5 at.% Ag suggests that the photoexcited electron-hole pairs are most effectively separated, which leads to the highest photocatalytic activity.

Thus, one may thus conclude that Ag coated ZnO nanospheres acts as an electron acceptor, which is beneficial to the effective separation of electron-hole pairs photogenerated in the ZnO and inhibits their recombination, thereby resulting in a stronger SPV response. In traditional noble-metal/oxide semiconductor composites, such as Pt/TiO₂ and Au/TiO₂, the noble metals have been demonstrated to serve as electron sinks for electrons generated in light-activated TiO₂, thereby leading to an improved quantum efficiency (Li et al. 2009). The role of Ag in our model system is similar to the noble metal.

Photocatalytic performance

Figure 9 shows the photocatalytic activities of pure ZnO nanoparticles and Ag/ZnO nanoparticle heterostructures for MO photodegradation. It can be seen that, after irradiation under UV light for 170 min, the concentration of the pure MO aqueous solution increases slightly owing to the evaporation of the water. This means that MO is sufficiently stable for the investigation of the photocatalytic activity of the Ag/ZnO composite nanocatalyst.

On the contrary, all Ag/ZnO nanocomposites exhibit much higher photocatalytic activity than pure

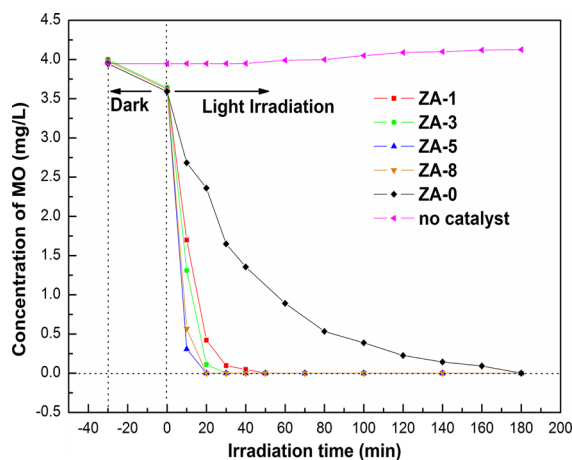


Fig. 9 The concentration changes of MO versus irradiation time

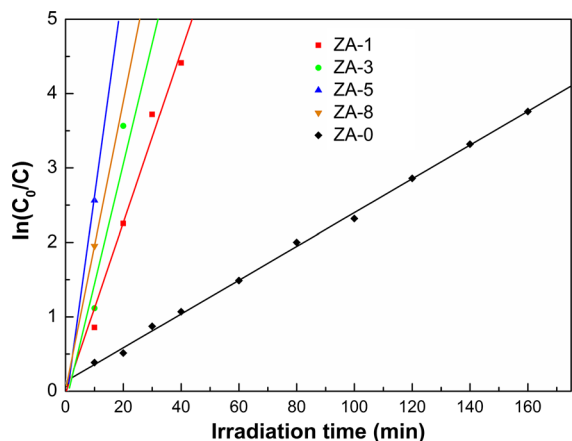


Fig. 10 First-order linear transforms quantifying the decomposition of MO by Ag/ZnO-assisted photocatalysis under UV irradiation

ZnO, with the ZA-5 sample showing the best performance. After 20 min, MO degradation reaches 100 %, while pure ZnO particles can only degrade 39 % of the pollutant dye.

The decomposition of MO under UV irradiation was fitted to the first order kinetic model. Figure 10 quantifies the decomposition rates of MO by Ag/ZnO-assisted photocatalysis under high-pressure mercury lamp. The rate constant values, fitting equations, and regression coefficients are summarized in Table 4. It is found that Ag/ZnO nanoparticle heterostructures with the Ag/Zn molar ratio of 5:95 (ZA-5) show the highest MO degradation efficiency which is approximately 11 times higher than that of pure ZnO.

It is well known that after irradiation with photons with the energy equal to or higher than the bandgap energy, the electrons in the valence band of ZnO can be excited into the conduction band, leading to the separation of electrons and holes as sketched in Fig. 11. These excited electrons can be further captured by O₂ to form superoxide radical anion

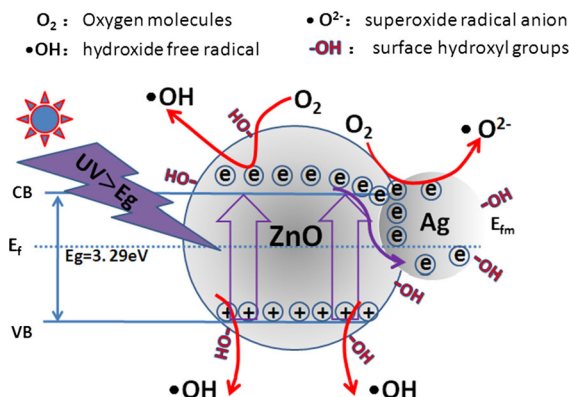


Fig. 11 Charge separation and the photocatalytic mechanism of the Ag/ZnO nanoparticle heterostructures under UV irradiation

(•O₂[−]), while the holes can be captured by OH[−] to form free hydroxide radical (•OH), which are reactive species contributing to the dye photodegradation.

The enhancement effect of Ag on the photocatalytic activity of ZnO is related to the change of Fermi energy levels of Ag and ZnO (Zheng et al. 2008; Chai et al. 2014; Saravanan et al. 2013). The Fermi energy level of Ag is higher than that of ZnO. When Ag and ZnO contact, some fraction of free electrons transfer from Ag to ZnO until the two systems attain a new and balanced Fermi energy level (E_f). However, the resulting E_f is still lower than the conduction band of ZnO.

Figure 11 explains the mechanism of photocatalytic action of the Ag/ZnO heterostructures. Because of the lower energy level of E_f, the excited electrons in the conduction band of ZnO can flow into Ag which can serve as a sink for excited electrons, thus facilitating the electron–hole segregation. As reported in “Photoluminescence spectra” section, the photocatalytic activity and PL intensity of the samples show the opposite variation trends with the change of the Ag

Table 4 Rate constants, fitting equations, and regression coefficients for MO degradation

Photo catalyst	Equation	Rate constant k (min ^{−1})	Regression coefficient R ²
ZA-0	y = 0.0227 * x + 0.10041	0.0227	0.99895
ZA-1	y = 0.1150 * x + 0.10965	0.1150	0.99303
ZA-3	y = 0.1735 * x + 0.23057	0.1735	0.97512
ZA-5	y = 0.2467 * x	0.2467	1.0
ZA-8	y = 0.1856 * x	0.1856	1.0

content. Indeed, the ZA-5 sample exhibits the highest photocatalytic activity, while its PL intensity is the weakest.

This finding confirms the role of the separation effects between photoinduced electrons and holes upon UV irradiation (Hong et al. 2013; Xin et al. 2005; Wang et al. 2013a, b, c). In general, the PL emission and the photocatalytic activity are related. For example, for Ag-loaded TiO₂ nanoparticles, the low PL intensity corresponds to the high photocatalytic activity due to the low excitonic PL caused by the separation of photoinduced electrons and holes (Yao et al. 2002). This mechanism is also relevant to the Ag/ZnO nanoparticle heterostructures of our interest here. The excited electrons both in the conduction band of ZnO and in Ag islands can be further captured by O₂ to form $\bullet\text{O}^{2-}$. This also contributes to the higher photocatalytic activity of Ag/ZnO under UV light compared with pure ZnO nanoparticles.

The results of photocatalytic performance in Fig. 9 also reveal that with the increasing Ag content, the photocatalytic activity of Ag/ZnO nanoparticle heterostructures first increases and then decreases. There are some reasons for this phenomenon. First, high crystallinity, large specific surface areas, the presence of hydroxyl groups on the surface of catalyst and suitable bandgap energy play a crucial role in the photocatalytic properties of semiconductor nanoparticles (Saravanan et al. 2013). The crystallite sizes of ZnO/Ag heterostructure also significantly increased with the amount of Ag nanoparticle loading (as can be seen in Table 2). It can be seen that the calculated crystallite sizes of all the Ag/ZnO heterostructures are much larger compared with pure ZnO except for the ZA-3 sample.

The increased crystallite sizes are accompanied by the higher crystallinity and smaller specific surface areas. When the silver content of the composites was above the optimum atomic percentage of Ag of 5 at.%, the size of the composite nanoparticles in sample ZA-8 was larger than in ZA-5, as evidenced by the XRD and SEM results. Increasing the grain size of the composite nanoparticles leads to the reduced specific surface areas. This may decelerate the photocatalytic process by providing fewer interfaces between the MO molecules and the Ag/ZnO catalysts (Yin et al. 2012; Zhang et al. 2014a, b; Bai et al. 2013).

Second, for the photocatalytic oxidation process, surface hydroxyl groups not only can easily capture

holes to form a free hydroxide radical ($\bullet\text{OH}$) but also can enhance O₂ adsorption to trap electrons and produce more free hydroxide radicals ($\bullet\text{OH}$) (Lu et al. 2008a, b; Gu et al. 2009). As documented in the literature (Sin et al. 2014), a large number of main active species including holes (h_{vb}^+), OH radicals ($\bullet\text{OH}$), and superoxide radical anions ($\bullet\text{O}^{2-}$) are involved in the photocatalytic process. Other authors (Zhu et al. 2014) emphasize that the $\bullet\text{O}^{2-}$ and $\bullet\text{OH}$ species play a major role in the photocatalytic degradation of organic dyes.

After irradiation by the light with energy equal to or higher than the bandgap, the electrons in the valence band of ZnO can be excited into the conduction band, leading to the separation of electrons and holes. These excited electrons can be further captured by O₂ to form superoxide radical anion ($\bullet\text{O}^{2-}$), while the holes can be captured by OH⁻ to form a free hydroxide radical ($\bullet\text{OH}$), which are active species for organic dyes photodegradation. Because of the lower energy level of E_f, the excited electrons in the conduction band of ZnO can flow into Ag which can serve as a sink for excited electrons, thus facilitating the electron-hole segregation. Under such conditions, the excited electrons that are present not only in the conduction band of ZnO but also in the Ag islands can be further captured by O₂ to form superoxide radical anion ($\bullet\text{O}^{2-}$). As a result, the photocatalytic activity of the catalysts is enhanced.

For the photocatalytic oxidation process, surface hydroxyl groups not only can easily capture holes to form free hydroxide radical ($\bullet\text{OH}$) but also can enhance O₂ adsorption to trap electrons and produce more free hydroxide radicals ($\bullet\text{OH}$) (Lu et al. 2008a, b; Gu et al. 2009). XPS results (Table 3) show that ZA-5 have more surface hydroxyl groups compared with ZA-8. The increase in the number of hydroxyl radicals of the photocatalyst surface leads to the further separation of photogenerated electrons and holes and also produces more free hydroxide radicals ($\bullet\text{OH}$). As a result, the photocatalytic activity of the catalysts is further enhanced which is attributed to abundant surface hydroxyl groups on the Ag/ZnO composite catalyst.

Third, Ag nanoparticles on the semiconductor surface act as electron sinks, which provide sites for accumulation of the photogenerated electrons thus improving the separation of electrons and holes. However, when excessive amounts of Ag nanoparticles

are loaded onto ZnO, the silver particles may act as recombination centers thereby decreasing the catalytic efficiency of the Ag/ZnO composite particles (Xu et al. 2008; Divband et al. 2013; Zhang and Mu 2007; Lu et al. 2008a, b).

Therefore, the interplay of these factors is critical to the activity of the photocatalysts. Indeed, the optimum amount of Ag nanoparticles is needed to enhance the photocatalytic activity of ZnO under UV light exposure. The optimum content of the Ag nanoparticles was found to be approximately 5.0 at.%. To investigate the stability of the photoactivity for the Ag/ZnO nanoparticle heterostructures with the Ag content of 5 at.%, cyclic photodecomposition experiments were carried out under the same experimental conditions. As shown in Fig. 12, the photocatalytic activity of Ag/ZnO did not exhibit any significant loss after ten consecutive photocatalytic cycles. Thus, the Ag/ZnO catalyst synthesized by our method is robust during photolysis, which could be due to its high crystallinity and well-structured heterojunction.

An interesting feature of Ag nanoparticles is the presence of a localized surface plasmon resonance (LSPR) in the visible spectral region, where losses near the resonance are low. This effect may be important for PL quenching and photocurrent enhancement of materials containing Ag. These resonances may, in particular, play a role in the degradation of hazardous chemicals under solar irradiation. These effects are outside the scope of this work which focuses on the photocatalytic activity of Ag/ZnO under UV irradiation.

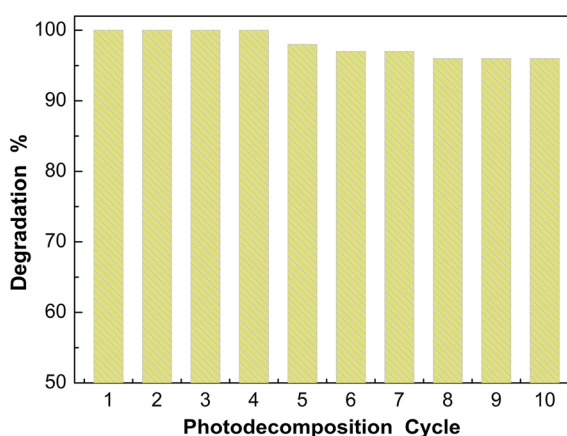


Fig. 12 Photocatalytic performance of the as-synthesized Ag/ZnO nanoparticle heterostructures with a Ag content of 5 at.% for the degradation of MO in 10 consecutive cycles (the reaction time for each cycle was 50 min)

Conclusion

In this work, Ag/ZnO nanoparticle heterostructures were prepared via a modified polymer-network gel route. Physical, chemical, and optical properties were analyzed using a range of analytic characterization techniques. XRD results demonstrate that the Ag/ZnO nanocomposites are composed of wurtzite ZnO nanoparticles and *fcc* Ag nanoparticles. SEM microscopy suggests that the powder is nearly spherical, polydisperse, and non-agglomerated. Moreover, the particle size is fairly uniform. The surface hydroxyl contents for Ag/ZnO composites increase first and then decrease, with the maximum content reached at 5 at.%. The intensity of PL for Ag/ZnO composites decreased first and then increased with the increasing amount of Ag nanoparticle loading. The best photocatalytic efficiency was demonstrated for the ZA-5 catalyst sample. In other words, 5 at.% of Ag is the optimum loading in the Ag/ZnO nanoparticle heterostructures, which not only separates the photoinduced electrons and holes, but also helps in producing the appropriate amount of the surface hydroxyl radicals to capture the charge carriers. The method is scalable, environment-friendly, and can potentially be used for other materials systems and applications in diverse fields which utilize catalytic effects.

Acknowledgments We would like to acknowledge the support by Sichuan Province academic and technical leader training fund (Grant No. 25727502) and the Subject Construction Funds of Southwest University for Nationalities (Grant No. 2015XWD-S0805), China. K. O. was partially supported by the Australian Research Council and CSIRO's Science Leadership Program. Assistance of S. Pineda in discussing and editing the manuscript is appreciated.

References

- Bai X, Wang L, Zon R, Lv Y, Sun Y, Zhu Y (2013) Performance enhancement of ZnO photocatalyst via a synergic effect of surface oxygen defect and grapheme hybridization. *Langmuir* 29:3097–3105
- Chai B, Wang X, Cheng S, Zhou H, Zhang F (2014) One-pot triethanolamine-assisted hydrothermal synthesis of Ag/ZnO heterostructure microspheres with enhanced photocatalytic activity. *Ceram Int* 40:429–435
- Dias MG, Azevedo EB (2009) Photocatalytic decolorization of commercial acid dyes using solar irradiation. *Water Air Soil Pollut* 204:79–87
- Dinesh VP, Biji P, Ashok A, Dhara SK, Kamruddin M, Tyagi AK, Raj B (2014) Plasmon-mediated, highly enhanced

- photocatalytic degradation of industrial textile dyes using hybrid ZnO@ Ag core-shell nanorods. *RSC Adv* 4:58930–58940
- Divband B, Khatamian M, Eslamian GK, Darbandi M (2013) Synthesis of Ag/ZnO nanostructures by different methods and investigation of their photocatalytic efficiency for 4-nitrophenol degradation. *Appl Surf Sci* 284:80–86
- Douy A (2001) Polyacrylamide gel: an efficient tool for easy synthesis of multicomponent oxide precursors of ceramics and glasses. *Int J Inorg Mater* 3:699–707
- Fockedey E, Van Lierde A (2002) Coupling of anodic and cathodic reactions for phenol electro-oxidation using three-dimensional electrodes. *Water Res* 36:4169–4175
- Galindo C, Jacques P, Kalt A (2001) Photooxidation of the phenylazonaphthol AO20 on TiO₂: kinetic and mechanistic investigations. *Chemosphere* 45:997–1005
- Georgeskutty R, Seery MK, Pillai SC (2008) A highly efficient Ag-ZnO photocatalyst: synthesis, properties, and mechanism. *J Phys Chem C* 112:13563–13570
- Gouvea CA, Wypych F, Moraes SG, Duran N, Nagata N, Peralta-Zamora P (2000) Semiconductor-assisted photocatalytic degradation of reactive dyes in aqueous solution. *Chemosphere* 40:433–440
- Gu C, Cheng C, Huang H, Wong T, Wang N, Zhang TY (2009) Growth and photocatalytic activity of dendrite-like ZnO@ Ag heterostructure nanocrystals. *Cryst Growth Des* 9:3278–3285
- Guo XH, Ma JQ, Ge HG (2013) Preparation, characterization, and photocatalytic performance of pear-shaped ZnO/Ag core-shell submicrospheres. *J Phys Chem Solids* 74:784–788
- Han A, Zhao M, Ye M, Liao J, Zhang Z, Li N (2013) Crystal structure and optical properties of YMnO₃ compound with high near-infrared reflectance. *Sol Energy* 91:32–36
- Hong Y, Tian C, Jiang B, Wu A, Zhang Q, Tian G, Fu H (2013) Facile synthesis of sheet-like ZnO assembly composed of small ZnO particles for highly efficient photocatalysis. *J Mater Chem A* 1:5700–5708
- Jing L, Qu Y, Wang B, Li S, Jiang B, Yang L, Fu W, Fu H, Sun J (2006) Review of photoluminescence performance of nano-sized semiconductor materials and its relationships with photocatalytic activity. *Sol Energy Mater Sol Cells* 90:1773–1787
- Kajbafvala A, Ghorbani H, Paravar A, Samberg JP, Kajbafvala E, Sadrnezhaad SK (2012) Effects of morphology on photocatalytic performance of Zinc oxide nanostructures synthesized by rapid microwave irradiation methods. *Superlattices Microstruct* 51:512–522
- Karunakaran C, Rajeswari V, Gomathisankar P (2011) Enhanced photocatalytic and antibacterial activities of sol-gel synthesized ZnO and Ag-ZnO. *Mater Sci Semicond Process* 14:133–138
- Khodja AA, Sehili T, Pilichowski JF, Boule P (2001) Photocatalytic degradation of 2-phenylphenol on TiO₂ and ZnO in aqueous suspensions. *J Photochem Photobiol A* 141:231–239
- Kositzki M, Antoniadis A, Poulous I, Kiridis I, Malato S (2004) Solar photocatalytic treatment of simulated dyestuff effluents. *Sol Energy* 77:591–600
- Kozlov DV, Paukshtis EA, Savinov EN (2000) The comparative studies of titanium dioxide in gas-phase ethanol photocatalytic oxidation by the FTIR in situ method. *Appl Catal B Environ* 24:L7–L12
- Li H, Wang D, Wang P (2009) Synthesis and studies of the visible-light photocatalytic properties of near-monodisperse bi-doped TiO₂ nanospheres. *Chem A Eur J* 15:12521–12527
- Lin GJ, Yang H, Xian T, Wei ZQ, Jiang JL, Feng WJ (2012) Synthesis of TbMnO₃ nanoparticles via a polyacrylamide gel route. *Adv Powder Technol* 23:35–39
- Liu X, Yang G, Fu S (2007) Mass synthesis of nanocrystalline spinel ferrites by a polymer-pyrolysis route. *Mater Sci Eng C* 27:750–755
- Lu W, Gao S, Wang J (2008a) One-pot synthesis of Ag/ZnO self-assembled 3D hollow microspheres with enhanced photocatalytic performance. *J Phys Chem C* 112:16792–16800
- Lu W, Liu G, Gao S, Xing S, Wang J (2008b) Tyrosine-assisted preparation of Ag/ZnO nanocomposites with enhanced photocatalytic performance and synergistic antibacterial activities. *Nanotechnology* 19:445711
- Ren C, Yang B, Wu M, Xu J, Fu Z, Guo T, Zhu C (2010) Synthesis of Ag/ZnO nanorods array with enhanced photocatalytic performance. *J Hazard Mater* 182:123–129
- Saravanan R, Karthikeyan N, Gupta VK, Thirumal E, Thangadurai P, Narayanan V, Stephen A (2013) ZnO/Ag nanocomposite: an efficient catalyst for degradation studies of textile effluents under visible light. *Mater Sci Eng C* 33:2235–2244
- Sauer T, Cesconeto Neto G, Jose HJ (2002) Kinetics of photocatalytic degradation of reactive dyes in a TiO₂ slurry reactor. *J Photochem Photobiol A* 149:147–154
- Sin JC, Lam SM, Satoshi I, Lee KT, Mohamed AR (2014) Sunlight photocatalytic activity enhancement and mechanism of novel europium-doped ZnO hierarchical micro/nanospheres for degradation of phenol. *Appl Catal B Environ* 148:258–268
- Su W, Zhang Y, Li Z (2008) Multivalency iodine doped TiO₂: preparation, characterization, theoretical studies, and visible-light photocatalysis. *Langmuir* 24:3422–3428
- Sun F, Qiao X, Tan F, Wang W, Qiu X (2012a) One-step microwave synthesis of Ag/ZnO nanocomposites with enhanced photocatalytic performance. *J Mater Sci* 47:7262–7268
- Sun F, Tan F, Wang W, Qiao X, Qiu X (2012b) Facile synthesis of Ag/ZnO heterostructure nanocrystals with enhanced photocatalytic performance. *Mater Res Bull* 47:3357–3361
- Tünay O, Kabdasi I, Eremektar G, Orhon D (1996) Color removal from textile wastewaters. *Water Sci Technol* 34:9–16
- Vanheusden K, Warren WL, Seager CH, Tallant DR, Voigt JA, Gnade BE (1996) Mechanisms behind green photoluminescence in ZnO phosphor powders. *J Appl Phys* 79:7983–7990
- Wang T, Wang H, Xu P, Zhao X, Liu Y, Chao S (1998) The effect of properties of semiconductor oxide thin films on photocatalytic decomposition of dyeing waste water. *Thin Solid Films* 334:103–108
- Wang J, Wang Z, Huang B, Ma Y, Liu Y, Qin X, Dai Y (2012a) Oxygen vacancy induced band-gap narrowing and enhanced visible light photocatalytic activity of ZnO. *ACS Appl Mat Interfaces* 4:4024–4030
- Wang S, Yu Y, Zuo Y, Li C, Yang J, Lu C (2012b) Synthesis and photocatalysis of hierarchical heteroassemblies of ZnO

- branched nanorod arrays on Ag core nanowires. *Nanoscale* 4:5895–5901
- Wang SF, Xiang X, Ding QP, Gao XL, Liu CM, Li ZJ, Zu XT (2013a) Size-controlled synthesis and photoluminescence of porous monolithic α -alumina. *Ceram Int* 39:2943–2948
- Wang SF, Xiang X, Sun G, Gao XL, Chen B, Ding QP, Zu XT (2013b) Role of pH, organic additive, and chelating agent in gel synthesis and fluorescent properties of porous monolithic alumina. *J Phys Chem C* 117:5067–5074
- Wang Y, Liu L, Xu L, Meng C, Zhu W (2013c) Ag/TiO₂ nanofiber heterostructures: highly enhanced photocatalysts under visible light. *J Appl Phys* 113:174311
- Wang SF, Lv HB, Zhou XS, Fu YQ, Zu XT (2014) Magnetic nanocomposites through polyacrylamide gel route. *Nanosci Nanotechnol Lett* 6:758–771
- Xian T, Yang H, Shen X, Jiang JL, Wei ZQ, Feng WJ (2009) Preparation of high-quality BiFeO₃ nanopowders via a polyacrylamide gel route. *J Alloys Compd* 480:889–892
- Xin B, Jing L, Ren Z, Wang B, Fu H (2005) Effects of simultaneously doped and deposited Ag on the photocatalytic activity and surface states of TiO₂. *J Phys Chem B* 109:2805–2809
- Xu J, Chang Y, Zhang Y, Ma S, Qu Y, Xu C (2008) Effect of silver ions on the structure of ZnO and photocatalytic performance of Ag/ZnO composites. *Appl Surf Sci* 255:1996–1999
- Yang Z, Zhang P, Ding Y, Jiang Y, Long Z, Dai W (2011) Facile synthesis of Ag/ZnO heterostructures assisted by UV irradiation: highly photocatalytic property and enhanced photostability. *Mater Res Bull* 46:1625–1631
- Yao BD, Chan YF, Wang N (2002) Formation of ZnO nanostructures by a simple way of thermal evaporation. *Appl Phys Lett* 81:757–759
- Yin X, Que W, Fei D, Shen F, Guo Q (2012) Ag nanoparticle/ZnO nanorods nanocomposites derived by a seed-mediated method and their photocatalytic properties. *J Alloys Compd* 524:13–21
- Zhang Y, Mu J (2007) One-pot synthesis, photoluminescence, and photocatalysis of Ag/ZnO composites. *J Colloid Interface Sci* 309:478–484
- Zhang M, Yang H, Xian T, Wei ZQ, Jiang JL, Feng YC, Liu XQ (2011) Polyacrylamide gel synthesis and photocatalytic performance of Bi₂Fe₄O₉ nanoparticles. *J Alloys Compd* 509:809–812
- Zhang X, Qin J, Xue Y, Yu P, Zhang B, Wang L, Liu R (2014a) Effect of aspect ratio and surface defects on the photocatalytic activity of ZnO nanorods. *Sci Rep* 4:4596
- Zhang Z, Liu H, Zhang H, Dong H, Liu X, Jia H, Xu B (2014b) Synthesis of spindle-like Ag/ZnO heterostructure composites with enhanced photocatalytic performance. *Superlattices Microstruct* 65:134–145
- Zheng Y, Zheng L, Zhan Y, Lin X, Zheng Q, Wei K (2007) Ag/ZnO heterostructure nanocrystals: synthesis, characterization, and photocatalysis. *Inorg Chem* 46:6980–6986
- Zheng Y, Chen C, Zhan Y, Lin X, Zheng Q, Wei K, Zhu J (2008) Photocatalytic activity of Ag/ZnO heterostructure nanocatalyst: correlation between structure and property. *J Phys Chem C* 112:10773–10777
- Zhu Y, Liu D, Lai Y, Meng M (2014) Ambient ultrasonic-assisted synthesis, stepwise growth mechanisms, and photocatalytic activity of flower-like nanostructured ZnO and Ag/ZnO. *J Nanopart Res* 16:1–13